Version of Record: https://www.sciencedirect.com/science/article/pii/S0254058416303339
Manuscript_076c3e05cc8063a3b71873eb3d056600

# Performance of HIPIMS deposited CrN/NbN nanostructured coatings exposed to 650°C in pure steam environment

P. Eh. Hovsepian[1]*, A.P. Ehiasarian[1], Y.P. Purandare[1], B. Biswas[1],
F.J. Pérez[2], M.I. Lasanta[2], M.T. de Miguel[2], A. Illana[2],
M. Juez-Lorenzo[3]
R. Muelas[4], A. Agüero[5],

[1]*UK National Technology HIPIMS Centre, Materials and Engineering Research Institute, Howard Street, Sheffield Hallam University, Sheffield, S1 1WB, UK.*

[2]*Grupo de Ingeniería de Superficies y Materiales Nanoestructurados. Facultad de Ciencias Químicas. Universidad Complutense de Madrid. 28040 Madrid, Spain*

[3] *Fraunhofer Institut für Chemische Technologie ICT, Joseph-von-Fraunhofer-Straße 7, 76327 Pfinztal, Germany*

[4] *Ingeniería de Sistemas para la Defensa de España SA, Beatriz de Bobadilla No. 3, Madrid, 28040 Spain*

[5] *Instituto Nacional de Técnica Aeroespacial (INTA), Ctra. Ajalvir Km. 4, 28850 Torrejón de Ardoz (Madrid), Spain*

* Corresponding author: Email: P.Hovsepian@shu.ac.uk. Telephone: +44-114-225 3644
Fax: +44-114-225 3501.

## Abstract

In the current work, 4 µm thick CrN/NbN coating utilising nanoscale multilayer structure with bi-layer thickness of Δ = 2.9 nm has been used to protect 9 wt. % Cr steels such as P92 widely used in steam power plants. The uniquely layered coatings have a combination of nitrides of chromium and niobium which are not only resistant to aqueous corrosion and corrosion-erosion and have excellent tribological properties, but also have oxidation resistance in dry air up to a temperature of 850°C. The novel High Power Impulse Magnetron Sputtering (HIPIMS) deposition technology has been used to deposit CrN/NbN with enhanced adhesion (critical load of scratch adhesion $L_{C2}$ = 80 N) and a very dense microstructure as demonstrated by Transmission Electron Microscopy (TEM) imaging. These superior coating properties are achieved due to the unique high metal ion content (up to 90%) in the HIPIMS plasma, which



© 2016 published by Elsevier. This manuscript is made available under the Elsevier user license
https://www.elsevier.com/open-access/userlicense/1.0/

allows particle acceleration and trajectory control by external electrical and magnetic fields thus delivering highly energetic material flux on the condensing surface.

P92 bare and coated samples were oxidised at 650 °C in 100% steam atmosphere up to 2000 h, in order to simulate the future operation conditions of steam turbines employed in power plants. The oxidation kinetics was evaluated by mass gain measurements. Under these conditions CrN/NbN provided reliable protection of the P92 steel. The paper also discusses the effect of growth defects and high temperature crack formation analysed by Scanning Electron Microscopy and Focused Ion Beam-Scanning Electron Microscopy techniques (SEM and FIB-SEM, respectively) on the high temperature corrosion resistance in pure steam atmosphere thus revealing the coatings potential failure mechanisms.

**Keywords:** Thin films, Nitrides, Nano structures, Sputtering.

## 1. Introduction:

The demand for new materials to be used in supercritical steam power plants for efficient and clean coal utilization is ever growing. A significant reduction of $CO_2$ emissions is expected by increasing the efficiencies of the steam turbines to $\eta > 50\%$ which can be achieved by moving from subcritical conditions (180 bar/540 $^oC$) to an ultra-supercritical regime of operation (300 bar/620-650$^oC$). However, there are important challenges faced by different steel components, related to higher temperatures such as material failure due to high temperature oxidation, and phenomenon such as creep and erosion caused by descaled fragments. Over the years considerable research has been done in finding solutions to the above problems in terms of employing protective surface layers [1, 2].

Protective surface layers based on oxides of Aluminium (Al) and Chromium (Cr) have been found effective but with some limitations. Their deposition techniques such as thermal spraying, slurry application and Chemical Vapour Deposition (CVD), including their

advantages and limitations have been concisely described in a previous publication [3]. Some of these coatings depend but also suffer from inter-diffusion of elements to and from substrate at high temperature which can compromise their density, leading to development of porosity eventually to substrate oxidation. It has also been reported that a critical amount of Cr and/or Al is required to form and maintain a protective oxide scale which will be effective at temperatures above 600 °C [4, 5]. Employing a surface layer with higher Cr or Al content [6] or nourish this layer with a constant supply of Cr from the layers beneath can be tricky in steels such as P92, since low Cr improves their creep resistance and thus their employability in the construction of steam plants [3, 7].

Literature studies have shown that so far the Physical Vapour Deposition (PVD) route has not been exploited to protect steam turbine components against the environmental attack caused by the steam at high temperature. The main reason is the porous structure of the state-of-the-art coatings, especially when monolithically grown, inherent to the growth mechanism of such coatings. In the current work, a surface coating however with a different approach has been studied. A PVD CrN/NbN coating utilising nanoscale multilayer, (superlattice) structure has been used to protect P92 steel. This uniquely layered coating is a combination of nitrides of chromium and niobium. Due to the plurality of the interfaces between the alternating individual layers, which act as barriers to the dislocation motion under mechanical load the hardness, and the toughness of the nanostructured coating are several factors higher than that of the individual single nitrides, which constitute the coating. Furthermore at exposure to high temperatures and aggressive environment the interfaces act as barriers to in and outward diffusion of coating, substrate as well as elements from the environment thus prolonging the coating life time against the environmental attack. CrN /NbN coatings which have excellent tribological properties and are not only resistant to aqueous corrosion and corrosion-erosion, [8, 9] but also have oxidation resistance up to a temperature of 850 °C [10], which further merits their use in the current study. Moreover, the novel High Power Impulse Magnetron

Sputtering (HIPIMS) deposition technology has been utilised to deposit these coatings with enhanced adhesion and very dense microstructure, which will address the problems of coating adherence at high temperature. These superior coating properties are achieved due to the unique high metal ion content in the HIPIMS plasma [11] which allows particle acceleration and trajectory control by external electrical and magnetic fields thus delivering highly energetic material flux on the condensing surface. The fundamentals and applications of this novel technology are described elsewhere [12]. The paper represents first attempt for more systematic study of the performance of HIPIMS deposited nanostructured coatings for the demanding application of steam turbines utilising unique steam environment testing equipment and advanced surface analytical techniques.

## 2. Experimental details:

### 2.1 Coating deposition:

Nanoscale multilayer CrN/NbN coatings were deposited in HTC 1000-4, four target system (Hauzer Techno Coatings, Europe B.V., Venlo, The Netherlands) enabled with HIPIMS technology at the UK National Centre for HIPIMS Technology at Sheffield Hallam University. The system is equipped with two HIPIMS power supplies (Hüttinger Elektronik Sp. z o.o., Warsaw, Poland). The industrial sized, computer controlled machine (chamber volume of $1m^3$) consists of a centrally placed rotating substrate table capable of three fold planetary rotation which helps in uniform coverage of complex 3D shaped components. The substrates can be suitably biased with the help of a dedicated bias power supply capable of handling highly ionised depositing flux (Hüttinger Elektronik Sp. z o.o., Warsaw, Poland). The system comprises of 4 rectangular cathodes which can be operated in Unbalanced Magnetron Sputtering (UBM) or High Power Impulse Magnetron Sputtering (HIPIMS) mode. Figure 1(a) shows the schematic cross-sectional view of the machine depicting the substrate

holder, arrangement of the cathodes and the closed magnetic field due to the external electromagnetic coils surrounding the magnets [13, 14].

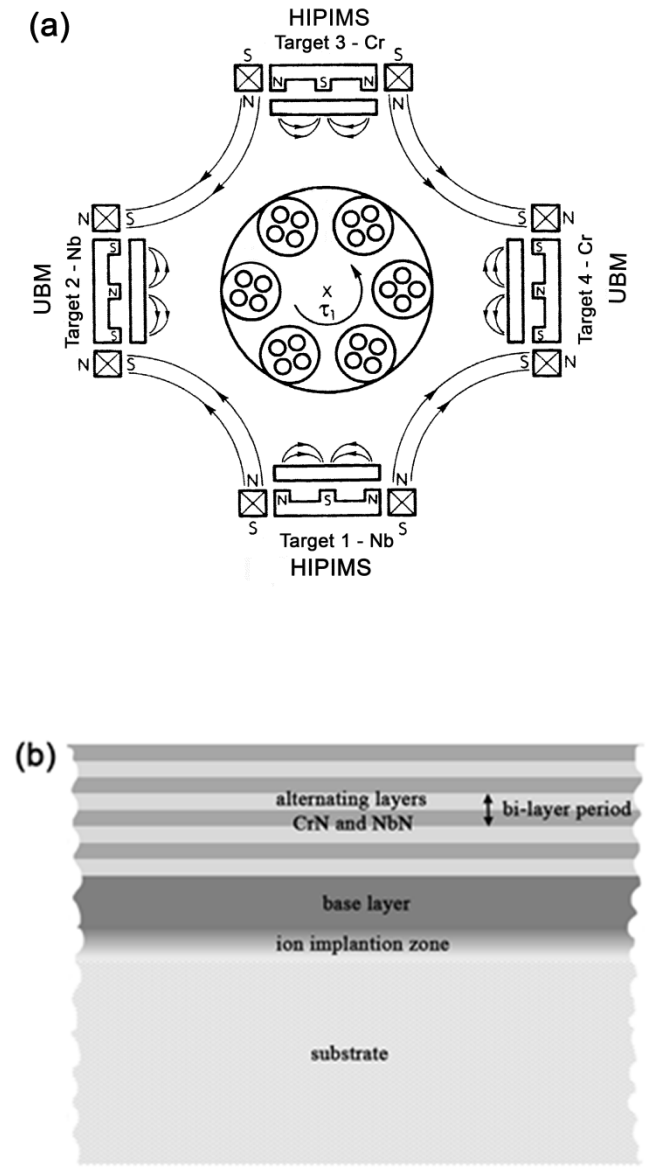



**Figure 1:** (a) schematic representation of the deposition chamber- HTC 1000-4 PVD coater (b) multilayer CrN/NbN coating architecture.

For this study P92 steel substrates with an engineering surface finish (clearly visible grinding marks-representing real engineering surfaces) were coated. CrN/NbN coatings were synthesised in a sequence of three steps – pre-treatment, CrN base layer deposition, and bulk

coating deposition comprising of nanoscale multilayer structure. Figure 1(b) shows the schematic of the coating architecture.

In order to improve adhesion of the coatings, substrates were pre-treated with $Cr^+$ produced in a HIPIMS plasma discharge operating in Ar atmosphere [15]. Pre-treatment was followed by a CrN base layer and then alternating CrN and NbN nanoscale layered architecture to form a multilayer coating by sequentially exposing the substrates placed on the substrate table to different targets. Two Nb and two Cr targets 99,90% pure were co-sputtered to deposit CrN/NbN coating. The sputtering was carried out in a mixed $N_2$+ Ar atmosphere at total pressure in the range of $10^{-3}$ mbar. The system was operated in a pressure control mode where the Ar flow rate was maintained constant of 200 sccm whereas the $N_2$ flow rate was varied in the range of 160-180 sccm using a VISCOVAC device and gas flow controllers. The primary rotation speed of the sample turn table was 7 rpm, which with the selected power on the targets and the nitrogen flow rate allowed deposition of nanoscale multilayer structured coating with bi-layer thickness of 2.9 nm. In order to achieve the desired combination of energy of the ionised flux and deposition rate, 2 targets were operated in HIPIMS and 2 in UBM mode [13]. The deposition temperature was maintained at 400 °C whereas the bias voltage ($U_b$) was maintained at -65 V.

**2.2 Coating characterisation:**

In order to investigate their performance, the coatings were characterised using a number of analytical techniques. Scanning Electron Microscopy (FEI NOVA-NANOSEM 200 and Zeiss Supra 55VP), Focussed Ion Beam SEM (Quanta 200 3D) were used to analyse the coating microstructures, whereas low-angle (2θ, 1°-10°) Bragg-Brentano geometry X-Ray Diffraction (XRD) technique was used to measure the bi-layer period of these coatings (PHILIPS XPERT). The texture of the nanoscale multilayer structure was investigated using Brag-Brentano geometry (2θ, 20-100°) XRD, using glancing angle (2° incidence) and θ-2θ

geometries. The coating samples were analysed by XRD after exposure using a Bruker AXS D8 Discover. A transmission electron microscope (Philips EM420) was used to analyse the multilayer structure in detail.

Coating adhesion was measured by Daimler Benz Rockwell indentation tests as well as progressive loading scratch tests conducted on CSEM-Anton Paar REVETEST. The Knoop hardness of the coatings was measured with a MITUTOYO microhardness tester using a load of 25 g (approx. 0.25 N).

### 2.3 Oxidation tests:

P92 substrates and coated samples were oxidised at 650 °C in 100% steam atmosphere up to 2000 h, in order to simulate the future operation conditions of steam turbines employed in power plants [16, 17, 18]. Figure 2 shows the experimental laboratory setup for the steam oxidation test procedure. The samples were put into a tubular horizontal furnace connected to a second furnace where the steam is generated from de-oxygenated water. The water is re-circulated by means of a peristaltic pump and a condenser assembled to the reservoir.

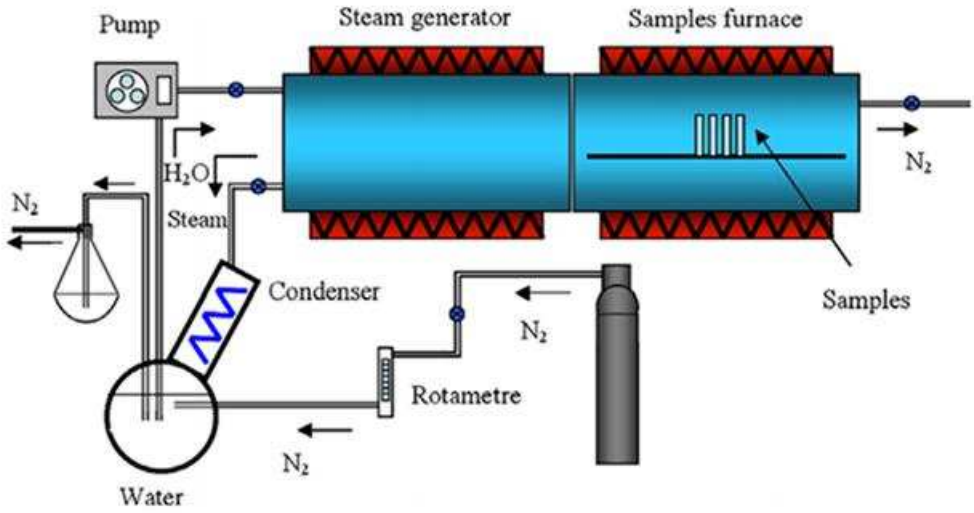



**Figure 2:** Schematics of the laboratory setup used for the steam oxidation tests [2].

The oxidation kinetics was evaluated by mass gain measurements in a five decimal balance. The specimens were removed from the chamber at fixed intervals. To prevent the oxidation of the samples while the furnace heats up to the test temperature or cools down to room temperature nitrogen gas was injected to displace the air from the chamber. Three coated and 3 uncoated specimens were oxidised to confirm the reproducibility of the data.

## 3. Results and discussion:

### 3.1 Coating mechanical properties and adhesion:

The effect of the coating superlattice structure on the properties is evident from the Knoop micro-hardness (HK) test results. A high value of $HK_{0.25N}$ = 3337 ± 83 (approximately 30 GPa) was measured which is a result of a dense, ordered and flat, (low waviness) nanolayer structure. Roughness values of the uncoated and coated P92 substrates (Ra = 0.65 µm and 0.70 µm respectively) were found to be near similar suggesting that HIPIMS coating does not add to the roughness due to any macro-sized defects such as droplets, but only follows closely the topography of the original surface. The roughness results reinforce the results obtained from SEM studies.

However as dense as the coating may be, its adhesion to the substrate is of paramount importance. To improve the adhesion of these coatings, the substrate surface was pre-treated with HIPIMS plasma. The utilisation of high energy metal ion rich plasma (typically few 100 eV), free from macro droplets, leads to very effective removal of any oxides/impurities present on the surface rendering it flat and clean. Furthermore the bombardment leads to metal ion implantation which promotes local epitaxial growth of the coating thereby improving adhesion. The fundamentals and further details of the adhesion enhancement due to the HIPIMS surface pre-treatment have been published elsewhere in [19].

Beneficial effect of HIPIMS pre-treatment and deposition is further evident from the adhesion test carried out on test coupons. Scratch adhesion tests on P92 test coupons were carried out

by scratching the sample with a diamond tip indenter under progressively increasing normal load conditions. The value of normal load at which coating de-lamination begins is observed under a microscope and recorded as the critical load of adhesion failure ($L_{C2}$). Results revealed a very high value of $L_{C2}$ = 80 N and are of significant importance considering the high surface roughness of the sample. Figure 3(a) shows the optical microscope image of the scratch along with the higher magnification insets. It can be observed that increasing loads lead to through thickness perforation of the coating but without delamination even though loads reached 80 N.

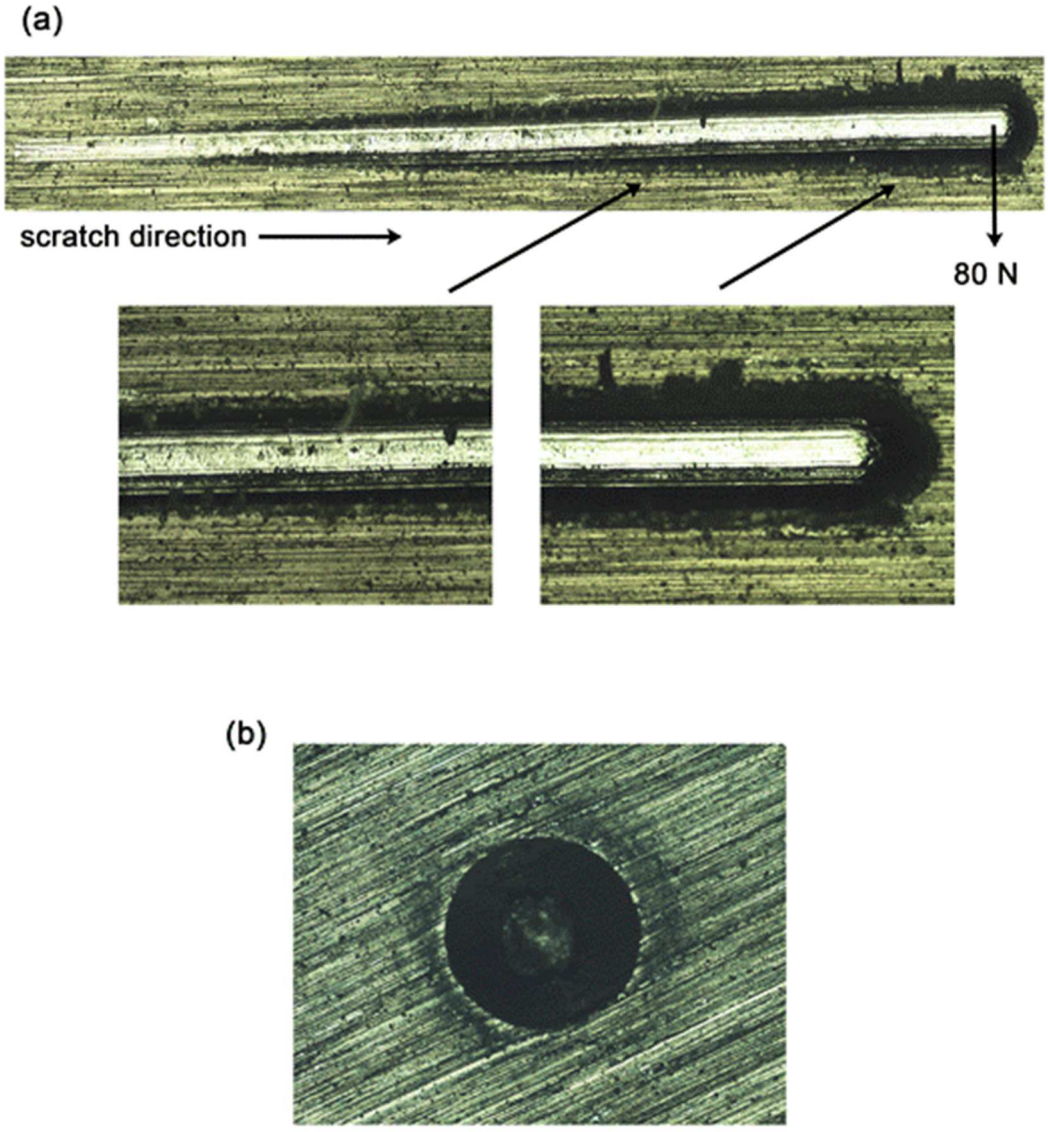



**Figure 3**: Optical images of (a) scratch adhesion test (b) Rockwell C, Daimler- Benz indentation test.

Figure 3(b) shows the optical images of Rockwell C indentation on the coated P92 substrate. Irrespective of the low hardness of the substrate material, the indentation is perfect without any coating de-lamination around the periphery and classifies as HF1 grade according to the Daimler-Benz adhesion test criteria.

### 3.2 Coating crystallographic structure and texture:

Performance of a coating in a hostile environment will largely depend on its microstructure along with its properties such as hardness, wear resistance, corrosion resistance and low internal stresses. These properties are influenced by the coating microstructure and texture to a large extent. A right combination: (a) of energetic flux generated in HIPIMS plasma and (b) application of a bias voltage, can act as a tool to control the texture in PVD coatings and thus their properties [20]. Intense low energy bombardment available in HIPIMS (positively charged particles typically with energies in the range of 2-3 eV) helps to mobilise the condensing species (material to be deposited) on the substrate surface. This in turn allows deposition of dense coatings however with lower stresses [13], and in case of multilayers with sharp interfaces leading to its superior properties [21].

XRD measurements revealed that the crystal structures of nanoscale CrN/NbN coating are a single phase FCC lattice, Figure 4(a). It was not possible to resolve individual reflections from CrN and NbN, which is typical for single phase nanoscale multilayer (superlattice) coatings where only one reflection appears located in the middle of the reflections of the pure nitrides. For example, the peak around $36^0$ is associated with CrN [111] reflection ($37.60^0$) and NbN [111] reflection ($35.36^o$). Results from the Brag-Brentano geometry configuration, Figure 4(a), indicate that the coatings had a pronounced (111) texture which is a low stress orientation [20]. Low Angle (1°-10°, 2Θ) X-Ray Diffraction (LAXRD) was used to reveal the superlattice structure of the coating. With CrN/NbN, a clear and sharp low angle reflections at $2\theta = 2.95°$ correspond to bi-layer period of $\Delta = 2.9$ nm Figure 4(b).

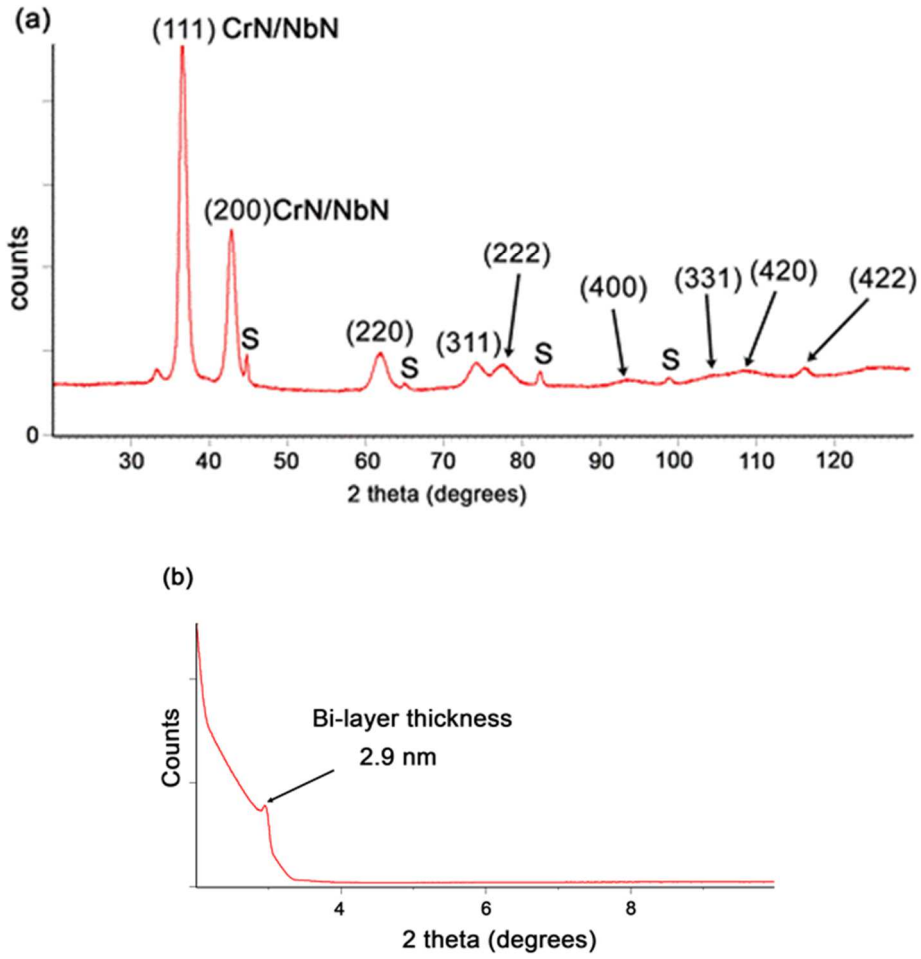



**Figure 4**: X-ray diffraction patterns of the CrN/NbN coating (a) Brag-Brentano Θ -2Θ scan, (b) LAXRD pattern used for calculation of the bi-layer period.

### 3.3 Coating morphology and microstructure:

***3.3.1 CrN/NbN surface morphology.*** Cross-sectional SEM studies on Si-samples, (image not shown here) revealed that the CrN/NbN coating had a total thickness of around 4 ± 0.20 µm. This includes the thickness of the CrN base layer of around 0.4 µm. The surface morphology of the coating has been analysed by low and high magnification SEM.

HIPIMS has been proven successful in depositing complex 3D components [22]. The highly ionised depositing species (both gas and metal ions) can be effectively guided to the "out of sight" areas with high kinetic energies when a bias voltage is applied to the substrate. This capability, when aided with 3 fold planetary rotation, improves the specimen coverage to a

large extent. This benefit of HIPIMS can also be observed in the current set of study, Figure 5 (a-c).

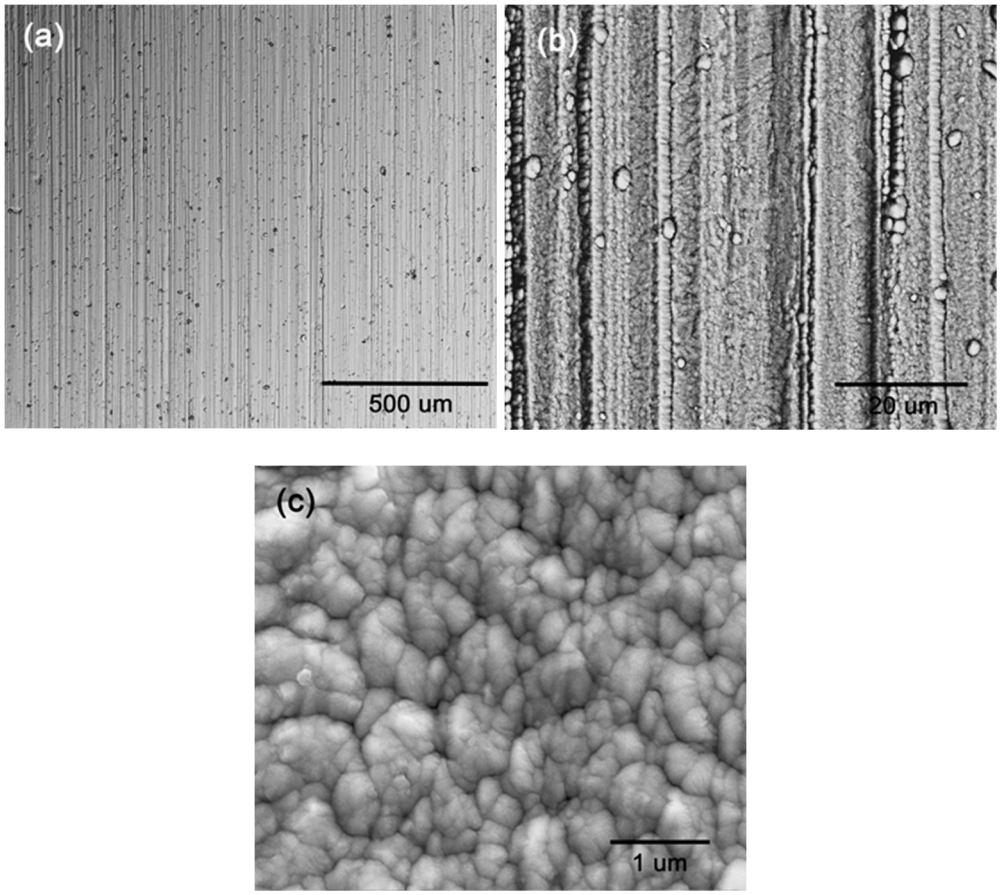



**Figure 5:** Scanning electron microscope images of CrN/NbN coating on P92 substrate: (a) lower magnification (b) coating surface at higher magnification (c) plan view of the dense columnar structure at nano level.

Figure 5(a) shows lower magnification image of the coated surface of a P92 specimen. In general surface appears uniformly coated without any macro-defects such as metal droplets often seen in technologies such as Arc evaporation. Thin PVD coatings, when deposited, usually conform the surface contours thereby preserving the original topography, in this case the groovy nature of the surface resulting from mechanical grinding. However, the beneficial effect of HIPIMS (ionised flux) can be clearly seen in Figure 5(b). The high magnification image shows that the peaks as well as the troughs of these groves have been fully coated.

Columnar grain sizes of the coating vary depending on its position (peaks show coarser diameter columnar grains than troughs) however the coating coverage is universal. The microstructure, consisting of multilayers when observed in cross-section, grows on the surface as several closely packed columnar grains. A higher magnification image in plan view shows the tops of the individual columns Figure 5(c). This peculiar structure often being referred as cauliflower structure further illustrates the coating density.

***3.3.2 CrN/NbN bulk coating microstructure***. The alternating CrN and NbN layered architecture of the CrN/NbN coating is achieved by sequential exposure of the substrate to different targets, (Cr and Nb) in the coating chamber as illustrated in section 2.1.

Figure 6(a, b) show the cross-sectional TEM images of the coating. Figure 6(a) shows the coating comprising a portion of the substrate, a CrN base layer followed by the bulk nano-layered CrN/NbN coating. The role of the CrN base or transition layer is to provide gradient in hardness and stress when transit from the soft substrate material, P92 into the very hard supelattice coating material. Such coating architecture further enhances the mechanical properties of the entire coating especially its adhesion. The benefit of HIPIMS etching is clearly evident; the substrate-coating interface is very flat and free from any amorphous oxide surface layers or macro-particle defects such as droplets. Also, large portions of the coating originating from the substrate are seen extended into the top of the coating (areas with similar contrast in the image) indicating local epitaxial growth. This ordered structure along with very dense coating, also evident in Figure 6(a), promotes high mechanical properties and adhesion of the coatings. Figure 6(b) shows a portion of the bulk of the multilayer coating. The multilayers appear flat, (low waviness) with sharp interfaces between the individual nano-layers, which further enhances the properties of the coating. It has to be mentioned that the sharpness of the image of the individual layers in the nanolayer structure depends on the crystal orientation and for bi-layer thicknesses below 3nm they are difficult to resolve.

Therefore the bi-layer thickness for the reported coatings is defined by two complementary methods, Low Angle XRD, Fig. 4 combined with XTEM imaging.

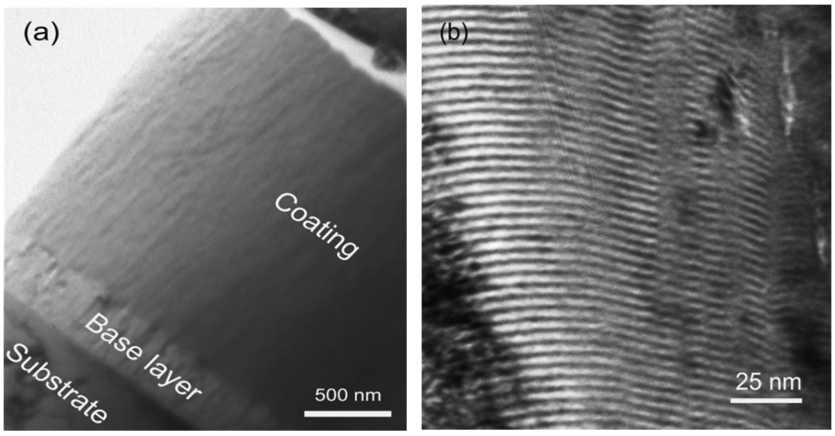



**Figure 6**: Bright field TEM (a) low magnification cross-section of the coating (b) high magnification showing the multilayers.

***3.3.3 Role of coating defects.*** The wear and corrosion resistance of the coating will strongly depend on its hardness, chemical inertness and thereby on its microstructure. Eventually coating structure defects will also play a vital role in the barrier, protection property provided by the coating. The structure defects are known to act as a preferential path of localised functionality coating failure [23, 24] and their effect will depend on their origin and their density. Therefore for the successful operation in the challenging environment of the steam turbine shedding light on the origin and the variety of the coating defects most commonly found is from paramount importance. One potential source of coating defects is the deposition technology itself. For example it is very common to form macro-particle droplet defects in the case of arc evaporation or under-dense microstructure leading to inter-columnar voids in the case of Direct Current (DC) sputtering. Defects can also develop during the condensation process when the coating grows on top of foreign particles which are ejected from deposition

chamber walls and fixtures and landed on the substrate surface. Figure 7(a-d) shows examples of such defects found on a PVD coated surface.

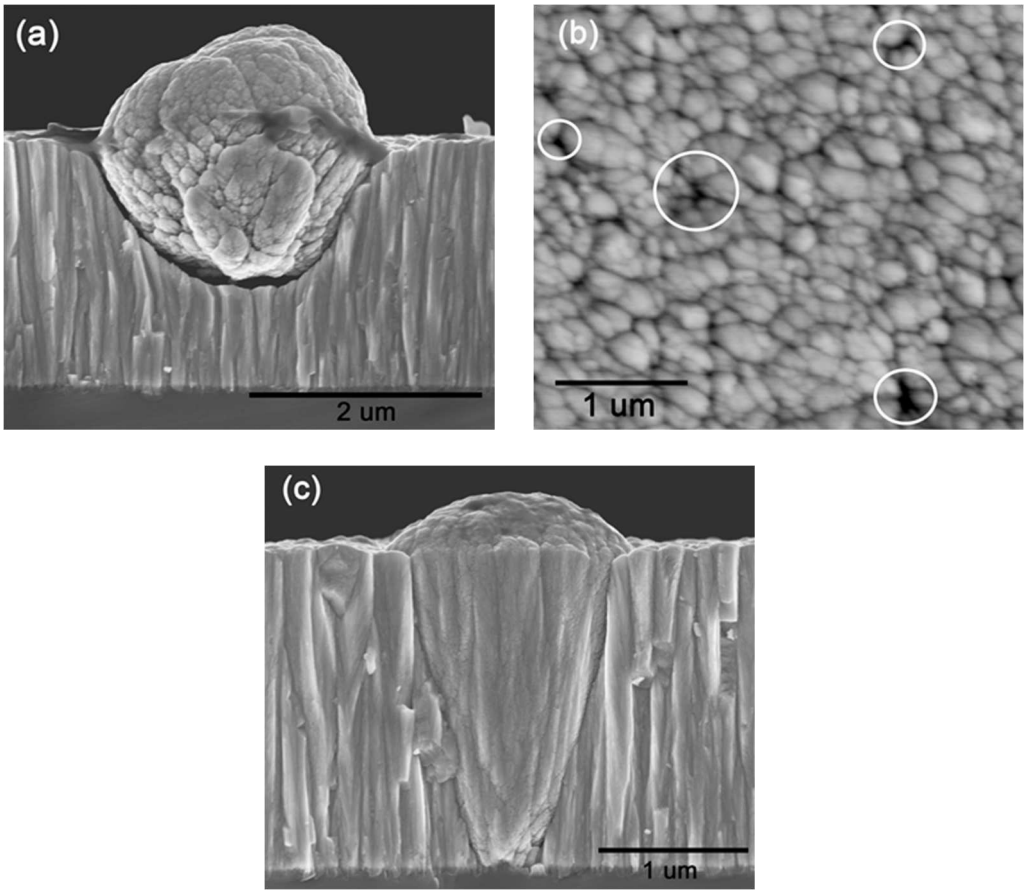



**Figure 7**: SEM images of various coating defects which can be found on a PVD coated surface (a) nodular defect (b) pin-hole defect (c) cone-like defect.

The observed coating defects can be roughly classified as:

*Nodular defects:* These appear as irregular shaped, loosely bond nodules of the coating, as visible in figure 7(a). These defects are generated by coating growth over foreign particles landed on the deposition surface at later stages of this process. The foreign particle causes shadowing, which creates under-dense areas (voids) under the defect and weakens the bond of the nodule to the surface and adjacent coating. These defects do not provide direct path from

the coating surface to the substrate therefore their existence is not seen as detrimental to the coating barrier properties in environmental tests, (in this study, steam corrosion test).

*Pin-hole defects:* Figure 7(b) is high magnification SEM image of a coating structure with a pinhole defect. These can be generated due to the defects on the substrate surface (such as small craters) leading to atomic shadowing effect during the condensation process resulting in formation of under-dense structures (voids). Most of the times these imperfections are small diameter voids and although they interconnect the coating surface with the substrate they get easily filled up with corrosion product at environmental exposure therefore are seen as less harmful to coating barrier property.

*Cone-like defects:* Figure 7(c) shows a cross sectional view of a coating with a cone like defect. These defects have a cone-like shape with a diameter reaching several microns. The origin of these defects is foreign or seed particles however, in contrast to the nodular defects the seed particles have been planted on the surface prior to the coating deposition or at very early stages of this process. The contact between the cone shape defect and the bulk of the coating is under dense with voids interconnecting the coating surface with the substrate. These types of defects are detrimental for the coating barrier properties as they act as primary sites for localised coating corrosion failure.

### 3.4 Oxidation test results:

As discussed before, the protective nature of the coating will largely depend on the inherent properties of the coating and on the microstructure of the coating. In order to analyse this CrN/NbN coated P92 substrates were subjected to oxidation tests at 650 °C for 2000 h in pure steam environment. Figure 8(a-c) shows the SEM images of the surface of the coated P92 substrate after oxidation tests. As seen in Figure 8(a); in general, the surface of the sample looks similar to the coated surface before oxidation tests (Figure 5) with no indication of coating spallation, of substrate oxidation or heavy built up of oxides even after 2000 h of

exposure. On closer inspection (Figure 8(b) and 8(c)) at higher magnification, the surface appears covered with very thin flake shaped features as well as nodules.

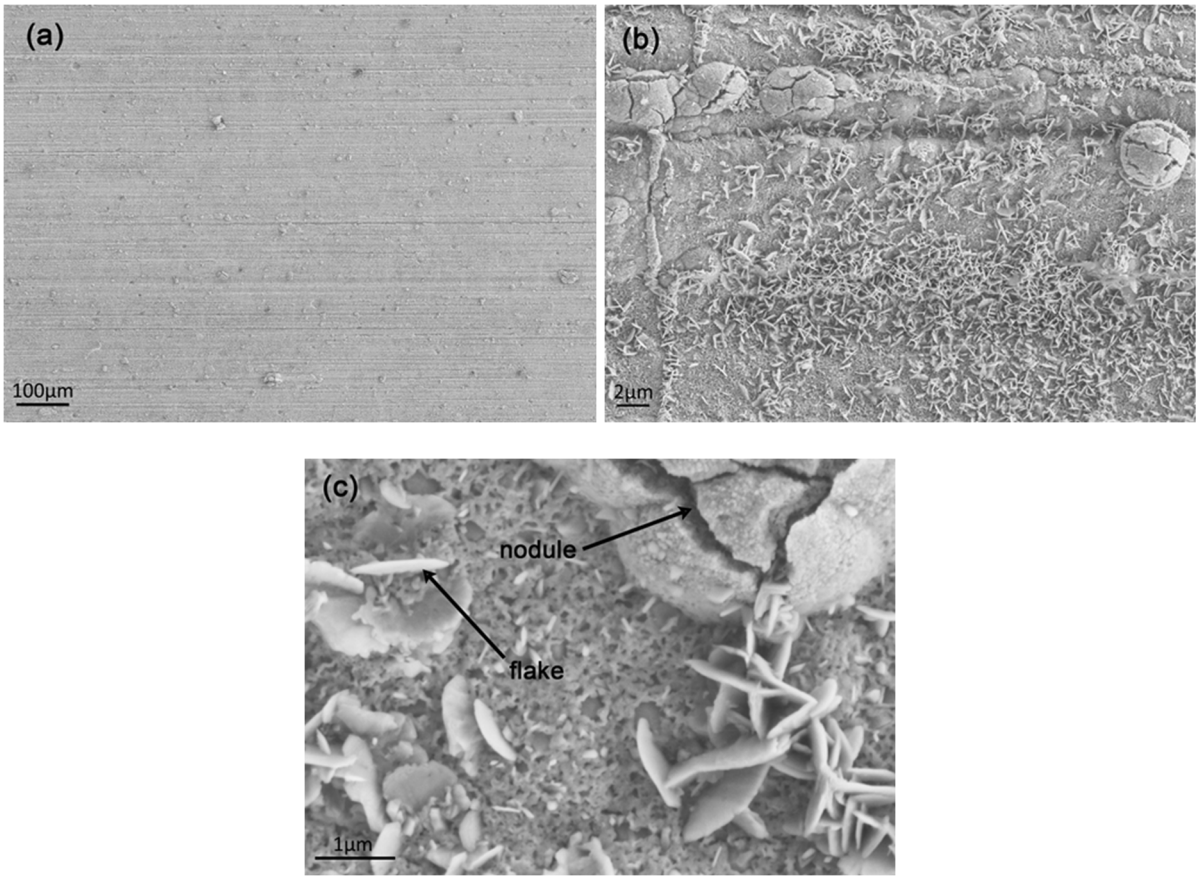



**Figure 8**: SEM images of the coating surface after oxidation tests (a) low magnification plan view of the surface (b) higher magnification focusing on the needle shaped oxides (c) higher magnification image of the oxides and cracked coating defect.

The surface is covered by a Cr and Nb rich oxide according to elemental analysis by EDX results shown in Figure 9. The flakes consist also of a Cr and Nb rich oxide but with lower Nb and tend to concentrate along machining marks as seen in Figure 9. This type of feature has already been observed by Quaddakers and collaborators [25], Agüero and collaborators [26], and is considered as evidence of fast Cr transport through oxides formed under water vapour containing atmospheres. The surface of the nodules is also covered by Cr and Nb oxides but some Fe and Mn can also be measured. This is confirmed by the XRD pattern of the coating

as shown in figure 9(b), in which peaks other than those corresponding to the substrate and the nitride coating, $Cr_2O_3$ and NbO as well as some $Fe_2O_3$ are seen. The nodules likely result from coating cone-like defects such as those described in section 3.3 and as observed in Figure 8(c), cracks appear on their surface likely due to geometrical effects as well as the difference in thermal expansion coefficients of the coating and the oxide.

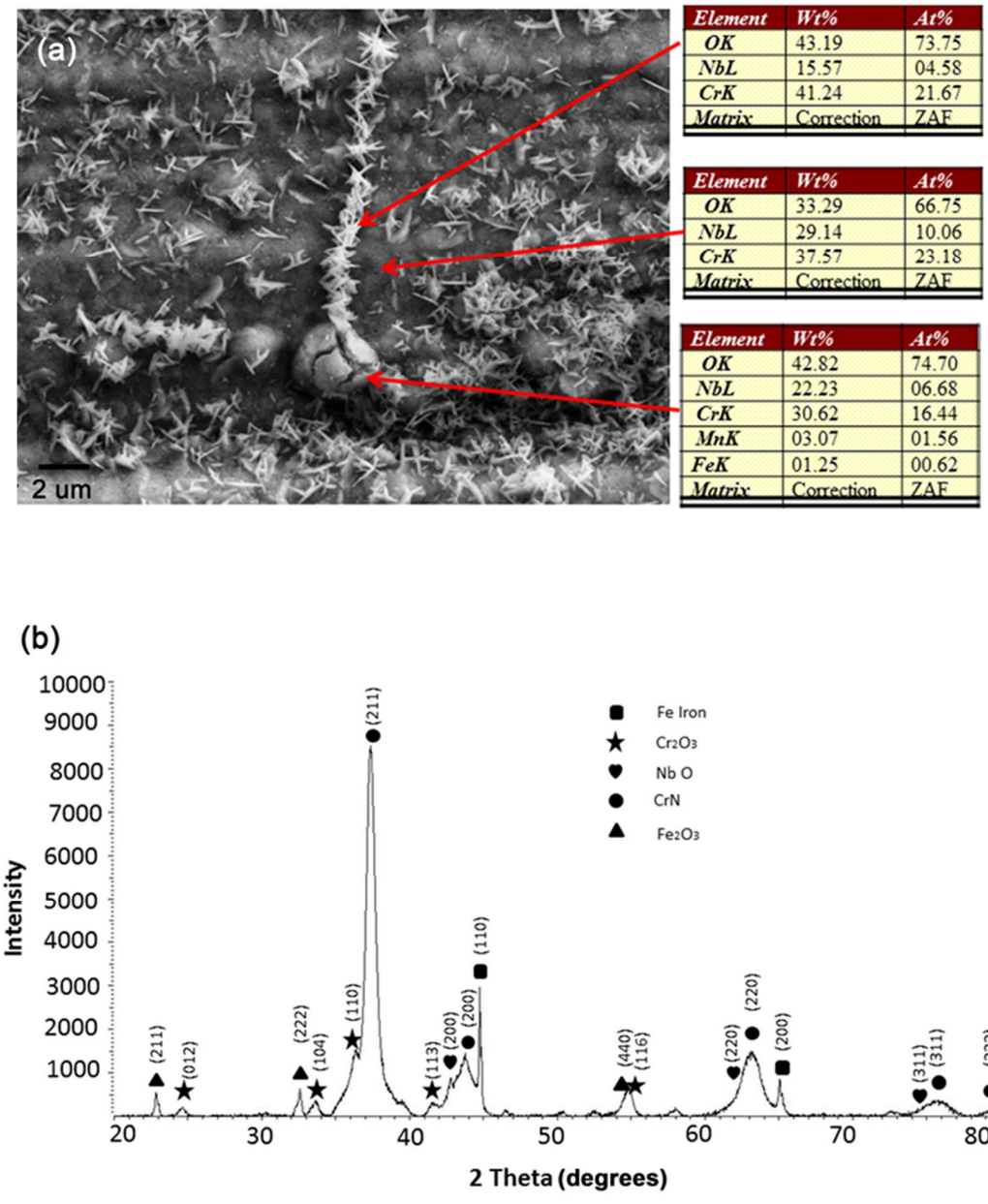



**Figure 9**: (a) SEM image of the coating surface after oxidation tests, insets show the elemental EDX analysis (b) XRD diffractogram of the coated surface after oxidation tests.

Figure 10 shows the cross-sectional SEM image of the CrN/NbN coating exposed to 2000 h of steam oxidation at 650 ºC. Through-thickness cracks can be observed and are likely due to thermal expansion coefficient mismatch between the coating and the substrate. Said cracks appear to get plugged by corrosion product; (oxides) therefore do not allow steam to reach the substrate causing its oxidation. Moreover, a nodule originating from a cone-like defect can be clearly observed surrounded by such cracks and covered by an oxide thicker than that of the rest of the surface. Through these cracks, Fe and Mn from the substrate can diffuse outwards and the presence of Fe in the oxide may cause faster growth. Chromium oxide is well known to be protective under the present conditions but the presence of Nb in high temperature protective oxides is not common.

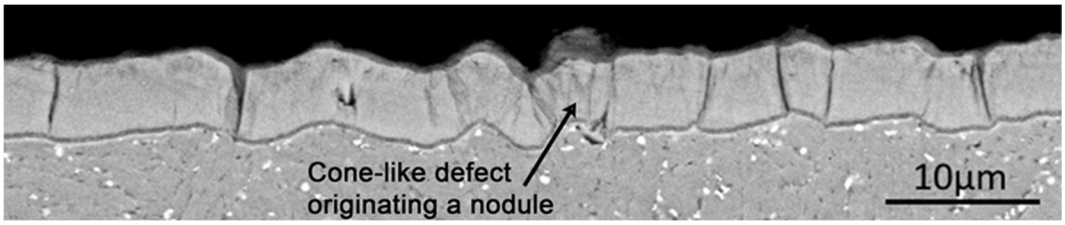


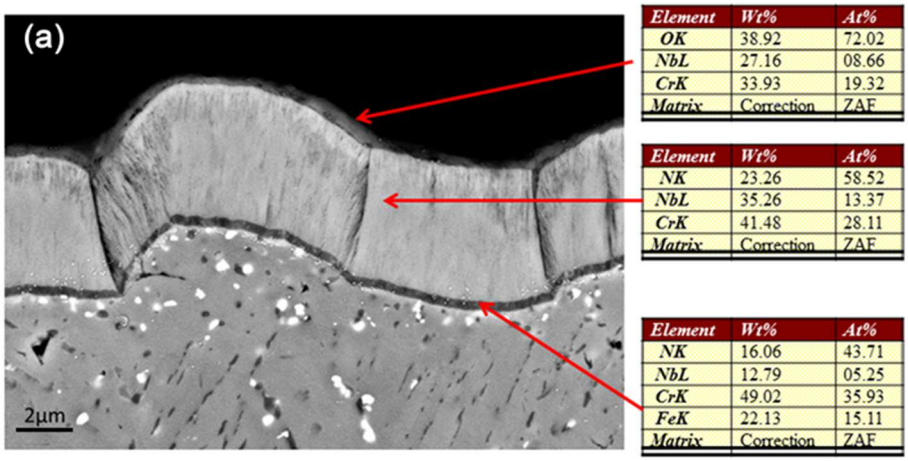

**Figure 10**: Cross-sectional back scattered SEM image of the coating cross-section showing cracks and a nodule.

In Figure 11, the elemental mapping as well as the composition of the coating shown. It can be clearly seen how the cracks are filled by protective oxides which prevent oxidation of the substrate. The fact that, neither substrate oxidation nor coating delamination can be observed indicates that the protective oxide formation is very fast. A thin oxide layer is also visible at the top of the coating (evident from the faint contrast in image and EDX analysis). Both SEM elemental mapping and EDX analyses carried out after 2000 hours of exposure to hostile high temperature steam environment showed that the coating developed a protective $Cr_2O_3$/NbO scale of approximately 490 nm. Chromium oxide is well known to be protective under the

presence conditions, whereas NbO is more effective at higher temperatures, (above 600º C) due to formation of a denser structure with a mildly protective nature [27, 28].

Furthermore, CrN/NbN coating architecture employed in the current study consisted of a CrN base layer which can be seen intact at the base of the coating in this cross-section image. It is clear from Figures 10 and 11(a) that the coating-substrate interface is still sharp and well defined. As anticipated, Cr, Nb and nitrogen is omnipresent throughout the coating thickness indicating the intact coating whereas oxygen can only been seen concentrated on the top or in the cracks suggesting its failure in penetrating through the coating cross-section. No decomposition of the coating has taken place and the coating has offered good protection against oxidation of the substrate.

Based on the above shown evidence the CrN/NbN coating protection mechanism can be described as one of formation of protective top Cr and Nb containing oxide layer, effective plugging of coating voids by oxide product as well as hindered elemental transport trough the coating due to the barrier properties of the interfaces between the individual nanolayers of the coating.



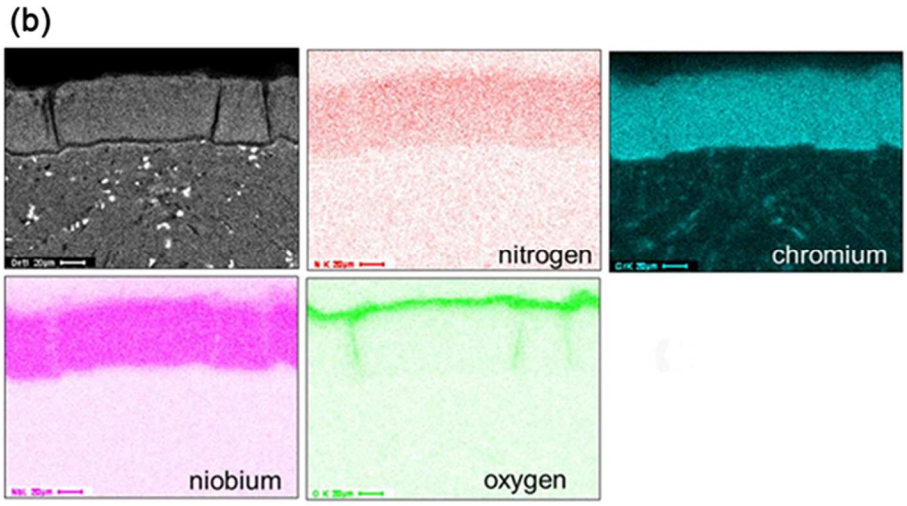



**Figure 11**: Cross-sectional back scattered SEM analysis (a) coating cross-section showing the coating and oxide layers on top with EDX analysis (b) Elemental mapping conducted on the cross-section.

In the current study, P92 substrates uncoated as well as coated with CrN/NbN were tested for their resistance against water steam attack. Figure 12 shows the results of this test. As observed CrN/NbN coated P92 substrate exhibits very small mass gain loss as compared to the uncoated substrate, which is known to develop thick oxide scales after short exposure [17]. The ≅ 200 nm thick protective oxide on top of a 4 microns thick coating appears exceptional as compared with other coatings, which need higher thickness and interact with the substrate causing degradation from both mechanical and oxidation resistance perspective [3].

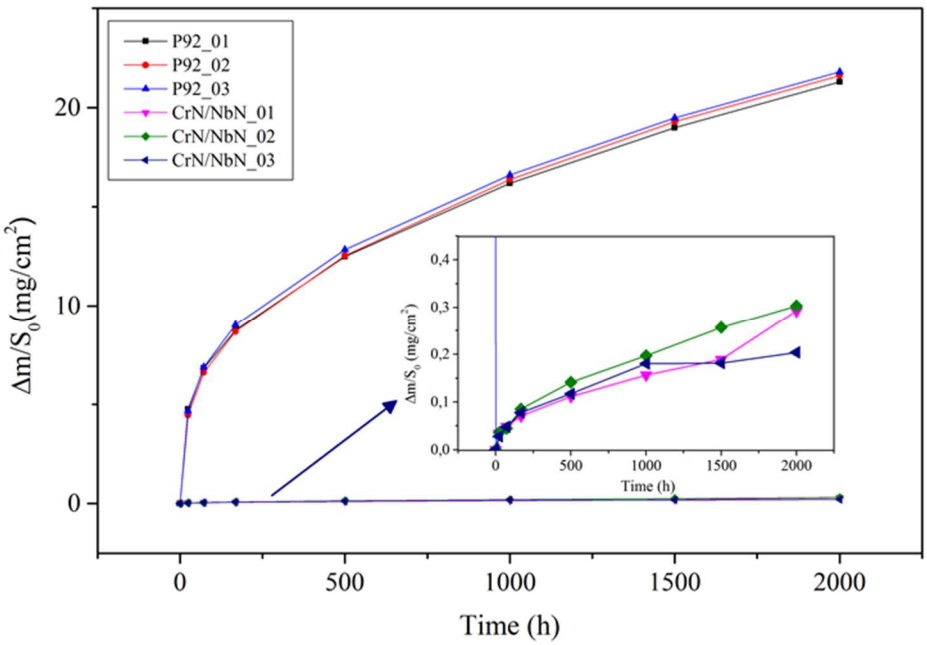



**Figure 12**: Mass gain as function of the test duration on exposure to 650 $^{o}$C in pure steam environment.

## 4. Conclusions

1. Wear resistant and electrochemically stable metals such as Cr and Nb were combined to produce CrN/NbN coating utilising superlattice structure with a bi-layer thickness of $\Delta$ = 2.9 nm. The novel technology providing highly ionised metal plasma, was successfully employed to deposit high hardness, $HK_{0.25N}$ = 3300 and extremely dense as shown by TEM coatings.

2. High adhesion with scratch test critical load of $L_{C2}$ = 80 N on P92 steel was achieved due to the use of the HIPMS surface pre-treatment, which modifies the substrate structure in such a way that local epitaxial growth of the condensing film occurs.

3. The coating degradation mechanism when exposed to high temperature steam environment, although retarded and localised, is adverse diffusion of substrate elements and oxygen through coating growth defects or cracks formed due to thermal expansion coefficient mismatch between the coating and the substrate.

4. SEM elemental mapping and EDX analyses carried out after 2000 h of exposure to hostile high temperature steam environment showed that the coating developed a protective

$Cr_2O_3$/NbO, whilst maintaining its original microstructure and phases and the coating-substrate interface remained sharp and well defined. The coating has offered good protection against oxidation of P92.

The coating protection mechanism can be described as one of formation of protective top Cr and Nb containing oxide layer, effective plugging of coating voids by oxide product as well as hindered elemental transport through the coating due to the barrier properties of the interfaces between the individual nanolayers of CrN/NbN.

**Acknowledgement**

This work has been carried out within FP7 EC funded project "Production of Coatings for New Efficient Clean Coal Power Plant Materials", POEMA, Grant agreement 310436. The financial support of the EC and the intellectual support of all partners are deeply acknowledged.

## References:

[1] F.J. Pérez, M.P. Hierro, J.A. Trilleros, M.C. Carpintero, L. Sánchez, J.M. Brossard, F.J. Bolívar, Iron aluminide coatings on ferritic steels by CVD-FBR technology, Intermetallics 14 (2006) 811-817.

[2] J. Leal, G. Alcalá, F.J. Bolívar, L. Sánchez, M.P. Hierro, F.J. Pérez., Simulation and experimental approach to CVD-FBR aluminide coatings on ferritic steels under steam oxidation, Corrosion Science 50 (2008) 1833-1840.

[3] A. Agüero, Progress in the development of coatings for protection of new generation steam plant components, Energy Materials 3 (2008) 35-44.

[4] A. Agüero, V. González, M. Gutiérrez, R. Muelas, Oxidation under pure steam: Cr based protective oxides and coatings, Surface & Coatings Technology 237 (2013) 30-38.

[5] F.J. Pérez, S. I. Castañeda, M.P. Hierro, R. Escobar-Galindo, J.C. Sánchez-López, S. Mato. Comparative study of micro- and nano-structured coatings for high-temperature oxidation in steam atmospheres, Oxidation of Metals 81 (2014) 227-236.

[6] S. Mato, G. Alcalá, M. Brizuela, R. Escobar-Galindo, F.J. Pérez, J.C. Sánchez-López, Long-term high temperature oxidation of CrAl(Y)N coatings in steam atmosphere, Corrosion Science 80 (2014) 453-460.

[7] A. Agüero, R. Muelas,V. Gonzalez, HVOF coatings for steam oxidation protection, Materials and Corrosion 59 (2008) 393-401.

[8] P.E. Hovsepian, D.B. Lewis, W.-D. Munz, A. Rouzaud, P. Juliet, Chromium nitride/niobium nitride superlattice coatings deposited by combined cathodic-arc/unbalanced magnetron technique, Surface & Coatings Technology 116–119 (1999) 727-734.

[9] Y.P. Purandare, A.P. Ehiasarian, M.M. Stack, P.Eh. Hovsepian, CrN/NbN coatings deposited by HIPIMS: A preliminary study of erosion-corrosion performance, Surface & Coatings Technology 204 (2010) 1158-1162.

[10] P.Eh. Hovsepian, D.B. Lewis, Q. Luo, W.-D. Münz, M. Meyer, High temperature performance of CrN/NbN superlattice coatings deposited on Ti-alloy substrates, Surface Engineering, Euromat Vol. 11 (1999) 41-46 proceedings, edited by H. Dimigen.

[11] A.P. Ehiasarian, A. Vetushka, A. Hecimovic, S. Konstantinidis, Ion composition produced by high power impulse magnetron sputtering discharges near the substrate, Journal of Applied Physics 104 (2008) nº 083305.

[12] A. Ehiasarian, "Fundamentals and applications of HIPIMS," in *Plasma surface engineering research and its practical applications*, R. Wei. Trivandrum, India, Research Signpost (2007) 35-86, ISBN 978-81-308-0257-2.

[13] P. Eh. Hovsepian, A.A. Sugumaran, Y. Purandare, D.A.L. Loch, A.P. Ehiasarian. Effect of the degree of high power impulse magnetron sputtering utilisation on the structure and properties of TiN films, Thin Solid Films 562 (2014) 132-139.

[14] Münz, W.-D., Schulze, D., and Hauzer, F.J.M. (1992). A new method for hard coatings: ABS™ (arc bond sputtering). Surface and Coatings Technology 50: 169-178.]

[15] A.P. Ehiasarian, P.Eh. Hovsepian, W-D. Münz, Combined coating process comprising magnetic field-assisted, high-power, pulsed cathode sputtering and an unbalanced magnetron, Patent US7081186 B2 (25 Jul 2006), EP1260603 A2 (27 Nov 2002), DE10124749 A1 (28 Nov 2002).

[16] A. Shirzadi, S. Jackson. Structural alloys for power plants: Operational challenges and high-temperature materials. ELSEVIER (2014) ISBN: 978-0-85709-238-0.

[17] K. Yin, S. Qiu, R. Tang, Q. Zhang, L. Zhang, Corrosion behavior of ferritic/martensitic steel P92 in supercritical water, The Journal of Supercritical Fluids 50 (2009) 235-239.

[18] A. Di Gianfrancesco, S.Tiberi Vipraio, D. Venditti, Long term microstructural evolution of 9-12% Cr steel grades for steam power generation plants, Procedia Engineering 55 (2013) 27-35.

[19] A.P. Ehiasarian, J.G. Wen, I. Petrov, Interface microstructure engineering by high power impulse magnetron sputtering for the enhancement of adhesion, Journal of Applied Physics 101 (2007) nº 54301.

[20] A.P. Ehiasarian, A. Vetushka, Y. Aranda-Gonzalvo, G. Sáfrán, L. Székely, P.B. Barna, Influence of high power impulse magnetron sputtering plasma ionization on the microstructure of TiN thin films. Journal of Applied Physics 109 (2011) nº 104314.

[21] P.Eh. Hovsepian, A.P. Ehiassarian, Y.P. Purandare, R. Braun, I.M Ross, Effect of high ion irradiation on the structure, properties and high temperature tribology of nanoscale CrAlYN/CrN multilayer coating deposited by HIPIMS-HIPIMS technique, Plasma Processes and Polymers 6 (2009)S118-S123.

[22] P.Eh. Hovsepian, A.P. Ehiasarian, I. Petrov, Structure evolution and properties of TiAlCN/VCN coatings deposited by reactive HIPIMS, Surface & Coatings Technology 257 (2014) 38-47.

[23] H.W. Wang, M.M. Stack, S.B. Lyon, P. Hovsepian, W-D. Münz, The corrosion behaviour of macroparticle defects in arc bond-sputtered CrN/NbN superlattice coatings, Surface & Coatings Technology 126 (2000) 279-287.

[24] Y. Purandare, M.M. Stack, P. Hovsepian, A study of the erosion–corrosion of PVD CrN/NbN superlattice coatings in aqueous slurries, Wear 259 (2005) 256–262.

[25] M. Hänsel, W.J. Quadakkers, D.J. Young, Role of water vapor in chromia-scale growth at low oxygen partial pressure, Oxidation of Metals 59 (2003) 285-301.

[26] A. Agüero, V. González, P. Mayr, K. Spiradek-Hahn, Anomalous steam oxidation behavior of a creep resistant martensitic 9 wt. % Cr steel, Materials Chemistry and Physics 141 (2013) 432-439.

[27] W.M.M. Huijbregts, M.J. Brabers, Oxidation of niobium and of niobium coated with aluminium in steam-air mixtures, Proceedings S.E.R.A.I. Journee internationales d'étude sur l'óxydation des metaux. Bruxelles (1965).

[28] T. Mukaibo, M. Kanno, M. Yamawaki, Oxidation Behavior of Nb and Nb-V Alloys, Journal of Nuclear Science and Technology 2 (1965) 516-524.

## List of figure captions

**Figure 1:** (a) schematic representation of the deposition chamber- HTC 1000-4 PVD coater (b) multilayer CrN/NbN coating architecture.

**Figure 2:** Schematics of the laboratory setup used for the steam oxidation tests [2].

**Figure 3**: Optical images of (a) scratch adhesion test (b) Rockwell C, Daimler- Benz indentation test.

**Figure 4**: X-ray diffraction patterns of the CrN/NbN coating (a) Brag-Brentano Θ -2Θ scan, (b) LAXRD pattern used for calculation of the bi-layer period.

**Figure 5:** Scanning electron microscope images of CrN/NbN coating on P92 substrate: (a) lower magnification (b) coating surface at higher magnification (c) plan view of the dense columnar structure at nano level.

**Figure 6**: Bright field TEM (a) low magnification cross-section of the coating (b) high magnification showing the multilayers.

**Figure 7**: SEM images of various coating defects which can be found on a PVD coated surface (a) nodular defect (b) pin-hole defect (c) cone-like defect.

**Figure 8**: SEM images of the coating surface after oxidation tests (a) low magnification plan view of the surface (b) higher magnification focusing on the needle shaped oxides (c) higher magnification image of the oxides and cracked coating defect.

**Figure 9**: (a) SEM image of the coating surface after oxidation tests, insets show the elemental EDX analysis (b) XRD diffractogram of the coated surface after oxidation tests.

**Figure 10**: Cross-sectional back scattered SEM image of the coating cross-section showing cracks and a nodule.

**Figure 11**: Cross-sectional back scattered SEM analysis (a) coating cross-section showing the coating and oxide layers on top with EDX analysis (b) Elemental mapping conducted on the cross-section.

**Figure 12**: Mass gain as function of the test duration on exposure to 650$^{o}$C in pure steam environment.